Inorganic Chemistry
Article

*Inorg. Chem.* **2010**, *49*, 457–467 **457**
DOI: 10.1021/ic901347p

# Steric Titration of Arylthiolate Coordination Modes at Pseudotetrahedral Nickel(II) Centers

**Swarup Chattopadhyay,[†] Tapash Deb,[†] Jeffrey L. Petersen,[‡] Victor G. Young Jr.,[§] and Michael P. Jensen*[,†]**

[†]*Department of Chemistry and Biochemistry, Ohio University, Athens, Ohio 45701,* [‡]*C. Eugene Bennett Department of Chemistry, West Virginia University, Morgantown, West Virginia 26506, and* [§]*X-ray Crystallographic Laboratory, Department of Chemistry, University of Minnesota, Minneapolis, Minnesota 55455*

Received July 10, 2009

Several derivatives of the pseudotetrahedral phenylthiolate complex $Tp^{Me,Me}$Ni-SPh (**1**), $Tp^{Me,Me-}$ = hydrotris(3,5-dimethyl-1-pyrazolyl)borate, were prepared incorporating substituted arylthiolates, including a series of *ortho*-substituted ligands $Tp^{Me,Me}$Ni-SR (R = 2,6-$Me_2C_6H_3$, **2**; 2,4,6-$Me_3C_6H_2$, **3**; 2,4,6-$^iPr_3C_6H_2$, **4**; and 2,6-$Ph_2C_6H_3$, **5**) and a series of *para*-substituted complexes (R = $C_6H_4$-4-OMe, **6**; $C_6H_4$-4-Me, **7**; and $C_6H_4$-4-Cl, **8**). The products were characterized by $^1$H NMR and UV−vis spectroscopy. Spectra of **6**−**8** were consistent with retention of a common structure across the *para*-substituted series with modest perturbation of the spectral features of **1** assisting their assignment. In contrast, spectra of **2**−**5** were indicative of a significant change in configuration across the *ortho*-disubstituted series. The structure of complex **5** was determined by X-ray crystallography and a distinctive arylthiolate ligation mode was found, in which the $N_3S$ ligand field was significantly distorted toward a sawhorse, compared to a more common trigonal pyramidal shape (e.g., **1**). Moreover, the arylthiolate substituent rotated from a vertical orientation co-directional with the pyrazole rings and disposed between two of them in **1**, to a horizontal orientation perpendicular to and over a single pyrazole ring in **5**. This reorientation is necessary to accommodate the large *ortho* substituents of the latter complex. The divergent Ni−S coordination modes result in distinct $^1$H NMR and electronic spectra that were rationalized by density functional theory (DFT) and time-dependent DFT (TD-DFT) calculations. These results demonstrate rich coordination chemistry for arylthiolates that can be elicited by steric manipulation at the periphery of pseudotetrahedral ligand fields.

## 1. Introduction

Active site nickel ions are found in a number of bacterial and archaebacterial enzymes that catalyze organometallic reactions, including $H_2$ oxidation,[1] methane synthesis,[2,3] $CO_2$ reduction, and acetate synthesis.[2,4,5] This enzymology is environmentally significant in the global carbon cycle,[2] and may also represent precedent for sustainable energy technologies.[6,7] Recent structural work has elucidated a variety of active sites for nickel, typically with low-coordinate ligand fields in non-classical geometries, valence and spin states, and with sulfur ligands and cofactors.[8] These structures pose questions regarding dynamics and reactivity of novel active sites. As small molecule modeling is an established paradigm to examine these questions, we are accordingly interested in developing coordination chemistry of paramagnetic nickel complexes with sulfur ligands.[9−11]

The initial focus of our efforts has been pseudotetrahedral arylthiolate complexes supported by tris(pyrazolyl)borates.[9] A key advantage afforded by these tripodal supporting ligands is the ability to add substituents to the facially tridentate pyrazole rings, enabling manipulation of electronic and steric properties of the ligand.[12] As the substituents are disposed "vertically" (i.e., perpendicular to the $N_3$ donor plane), a pocket is formed about a fourth binding site for a

*To whom correspondence should be addressed. E-mail: jensenm@ohio.edu.

(1) Fontecilla-Camps, J. C.; Volbeda, A.; Cavazza, C.; Nicolet, Y. *Chem. Rev*. **2007**, *107*, 4273–4303.
(2) Ragsdale, S. W. *J. Inorg. Biochem*. **2007**, *101*, 1657–1666.
(3) Ermler, U. *Dalton Trans*. **2005**, 3451–3458.
(4) Jeoung, J.-H.; Dobbek, H. *Science* **2007**, *318*, 1461–1464.
(5) Drennan, C. L.; Doukov, T. I.; Ragsdale, S. W. *J. Biol. Inorg. Chem*. **2004**, *9*, 511–515.
(6) Smith, M. C.; Barclay, J. E.; Davies, S. C.; Hughes, D. L.; Evans, D. J. *Dalton Trans*. **2003**, 4147–4151.
(7) Benson, E. E.; Kubiak, C. P.; Sathrum, A. J.; Smieja, J. M. *Chem. Soc. Rev*. **2009**, *38*, 89–99.
(8) Maroney, M. J. *Curr. Opinion. Chem. Biol*. **1999**, *3*, 188–199.
(9) Chattopadhyay, S.; Deb, T.; Ma, H.; Petersen, J. L.; Young, V. G., Jr.; Jensen, M. P. *Inorg. Chem*. **2008**, *47*, 3384–3392.
(10) Ma, H.; Chattopadhyay, S.; Petersen, J. L.; Jensen, M. P. *Inorg. Chem*. **2008**, *47*, 7966–7968.
(11) Ma, H.; Wang, G.; Yee, G. T.; Petersen, J. L.; Jensen, M. P. *Inorg. Chim. Acta* **2009**, *362*, 4563–4569.
(12) Trofimenko, S. *Chem. Rev*. **1993**, *93*, 943–980.


Published on Web 12/15/2009

co-ligand. This effect enables rudimentary control of co-ligand bonding through steric contact, in modest analogy to typically elegant allosteric active site control achieved in metalloenzymes through all levels of protein structure.

We previously observed that the relatively large substituents of hydrotris(3-phenyl,5-methylpyrazolyl)borate (i.e., $Tp^{Ph,Me}$) forced significant bending of a Ni(II)-SAr bond; the observed bond angle increased from 103.84(8)° for $Tp^{Me,Me}$Ni-SPh (**1**) to 116.51(7)° for $Tp^{Ph,Me}$Ni-S-2,6-$Me_2C_6H_3$ (**9**) in respective X-ray crystal structures.[9] The arylthiolate coordination was otherwise quite similar in the two complexes, with the thiophenolate sulfur displaced off the 3-fold axis toward one pyrazole, and the aryl substituent oriented vertically (i.e., aligned between 3-substituents on the other two pyrazole rings). Several related complexes of various tripodal borate ligands have been reported. Similar vertical geometries were observed for $Tp^{iPr,iPr}$Ni-$SC_6F_5$,[13] an analogous tripodal borate complex with thioether donors,[14] and its $C_6H_5S^-$ congener.[14] In contrast, a tripodal borate with diphenylphosphinomethyl donor arms yielded a different motif, with the sulfur atom disposed between donors and the substituent significantly rotated toward horizontal,[15] as typically found for complexes with planar tetradentate supporting ligands.[16] Another class of $[Ni(SAr)_4]^{2-}$ complexes exhibits tetragonal ($D_{2d}$) distortion,[17−20] and a linear $Ni(SAr)_2$ complex has also been reported.[21] The distinctive features of these structures demonstrate disparate coordination modes for arylthiolates in pseudotetrahedral Ni(II) complexes.

In the present work, we probed arylthiolate ligation at $Tp^{Me,Me}Ni^{II}$ centers by selectively modifying the arylthiolate on the parent $Tp^{Me,Me}$Ni-SPh complex (**1**), either with increasingly bulky *ortho* groups (**2**−**5**), or with electronically significant *para* substituents (**6**−**8**). These complexes demonstrate a primary role for steric interaction with the tris(pyrazolyl) pocket in eliciting two disparate arylthiolate bonding modes, which have been structurally characterized and distinguished by spectroscopy and density functional theory (DFT) calculations.

## 2. Experimental Methods

**2.1. General and Synthetic Procedures.** All manipulations were carried out under an inert atmosphere of prepurified argon, either in a glovebox (MBraun Unilab) or using Schlenk techniques. $^1$H NMR data were recorded on a Varian Unity 500 spectrometer and processed using the MestReNova 5.1.0 software suite (Mestrelab Research, Santiago de Compostela, Spain); spectra were referenced internally to residual solvent. Solution magnetic moments were determined by the Evans NMR method in $CDCl_3$ at 295 K.[22] UV−visible−NIR spectra were recorded on an Agilent HP-8453 diode-array spectrophotometer. Elemental analyses were performed by Atlantic Microlabs, Inc. (Norcross, GA). $Tp^{Me,Me}$NiCl was prepared by metathesis of anhydrous $NiCl_2$ and $TlTp^{Me,Me}$ in MeOH/$CH_2Cl_2$ (***Caution****: thallium salts are extremely toxic and must be properly handled and disposed of*).[23] 2,6-Diphenyl- and 2,4,6-tris(isopropyl)phenylthiol were prepared by literature procedures,[24−26] and other thiols were obtained from a commercial vendor (Aldrich). The thiols were converted to respective sodium salts by titration of $NaNH_2$ in toluene, and reacted with $Tp^{Me,Me}$NiCl in tetrahydrofuran (THF) to obtain target complexes in 65−80% yields following toluene extraction as previously described.[9] Characterizations of product complexes are summarized below. All other materials were obtained from commercial vendors as ACS reagent-grade or better and used as received, except for drying of solvents by routine techniques.

**$Tp^{Me,Me}$Ni-$SC_6H_5$ (1).**[9] Anal. Calcd (found) for $C_{21}H_{27}BN_6NiS$: C, 54.23 (54.64); H, 5.85 (5.98); N 18.07 (18.24). UV−vis ($CH_2Cl_2$, $\lambda_{max}$, nm; $\varepsilon$, $mM^{-1}$ $cm^{-1}$): 354 (1.6); 464 (2.4); 506 (2.6); 614 (sh, 0.2); 836 (0.2); 970 (sh, 0.1). $^1$H NMR ($CDCl_3$, 295 K; $\delta$, ppm): 77.2 (3H, 4-pz); 23.3 (2H, *meta*); 6.6 (9H, 5-Me); −7.1 (9H, 3-Me); −10.7 (1H, B-*H*); −18.9 (2H, *ortho*); −26.6 (1H, *para*); $\mu_{eff}$ = 2.92 $\mu_B$.

**$Tp^{Me,Me}$Ni-S-2,6-$Me_2C_6H_3$ (2).** Anal. Calcd (found) for $C_{23}H_{31}BN_6NiS\cdot H_2O$: C, 54.05 (54.24); H, 6.51 (6.71); N 16.44 (16.57). UV−vis (toluene, $\lambda_{max}$, nm; $\varepsilon$, $mM^{-1}$ $cm^{-1}$): 342 (0.9); 368 (0.9); 411 (1.1); 471 (sh, 1.4); 511 (2.2); 640 (0.2); 856 (0.1); 958 (0.1). $^1$H NMR ($CDCl_3$; $\delta$, ppm): 75.3 (3H, 4-pz); 31.7 (6H, *ortho*); 25.2 (2H, *meta*); 5.5 (9H, 5-Me); −7.5 (9H, 3-Me); −10.4 (1H, *para*); −11.3 (1H, B-*H*).

**$Tp^{Me,Me}$Ni-S-2,4,6-$Me_3C_6H_2$ (3).**[9] Anal. Calcd (found) for $C_{24}H_{33}BN_6NiS$: C, 56.84 (56.75); H, 6.56 (6.59); N 16.57 (17.32). UV−vis ($CH_2Cl_2$, $\lambda_{max}$, nm; $\varepsilon$, $mM^{-1}$ $cm^{-1}$): 343 (1.1); 371 (1.1); 406 (1.2); 467 (sh, 1.5); 514 (2.7); 636 (sh, 0.2); 861 (0.2). $^1$H NMR ($CDCl_3$; $\delta$, ppm): 75.0 (3H, 4-pz); 33.3 (6H, *ortho*); 25.8 (3H, *para*); 25.3 (2H, *meta*); 5.2 (9H, 5-Me); −7.5 (9H, 3-Me); −11.3 (1H, B-*H*); $\mu_{eff}$ = 3.01 $\mu_B$.

**$Tp^{Me,Me}$Ni-S-2,4,6-$^i$Pr$_3C_6H_2$ (4).** Anal. Calcd (found) for $C_{30}H_{45}BN_6NiS$: C, 60.94 (61.03); H, 7.67 (7.83); N 14.21 (14.25). UV−vis ($CH_2Cl_2$, $\lambda_{max}$, nm; $\varepsilon$, $mM^{-1}$ $cm^{-1}$): 338 (sh, 1.1); 414 (2.2); 516 (2.8); 665 (0.3); 870 (0.2); 954 (0.1). $^1$H NMR ($CDCl_3$; $\delta$, ppm): 75.3 (3H, 4-pz); 24.5 (2H, *meta*); 19.7 (2H, 2,6-C*H*$Me_2$); 8.8 (1H, 4-C*H*$Me_2$); 8.0 (12H, 2,6-CH*Me*$_2$); 5.3 (9H, 5-Me); 2.3 (6H, 2,6-CH*Me*$_2$); −8.1 (9H, 3-Me); −11.8 (1H, B-*H*).

**$Tp^{Me,Me}$Ni-S-2,6-$Ph_2C_6H_3$ (5).** Anal. Calcd (found) for $C_{33}H_{35}BN_6NiS$: C, 64.21 (64.27); H, 5.72 (5.79); N 13.62 (13.57). UV−vis ($CH_2Cl_2$, $\lambda_{max}$, nm; $\varepsilon$, $mM^{-1}$ $cm^{-1}$): 357 (sh, 0.8); 422 (1.8); 516 (1.8); 657 (0.3); 867 (0.2); 942 (0.1). $^1$H NMR ($CDCl_3$; $\delta$, ppm): 76.5 (3H, 4-pz); 24.6 (2H, *meta*); 15.1 (4H, 2,6-*ortho*); 7.4 (2H, 2,6-*para*); 6.8 (4H, 2,6-*meta*); 5.9 (9H, 5-Me); 1.4 (1H, *para*); −9.4 (9H, 3-Me); −11.7 (1H, B-*H*); $\mu_{eff}$ = 2.89 $\mu_B$.

**$Tp^{Me,Me}$Ni-S-$C_6H_4$-4-$OCH_3$ (6).** Anal. Calcd (found) for $C_{22}H_{29}BN_6NiOS$: C, 53.37 (53.46); H, 5.90 (5.89); N 16.98 (17.21). UV−vis ($CH_2Cl_2$, $\lambda_{max}$, nm; $\varepsilon$, $mM^{-1}$ $cm^{-1}$): 348 (1.8); 484 (sh, 2.4); 517 (3.1); 843 (0.2); 1000 (sh, 0.1). $^1$H NMR ($CDCl_3$; $\delta$, ppm): 75.5 (3H, 4-pz); 22.5 (2H, *meta*); 6.3 (9H, 5-Me); −6.9 (9H, 3-Me); −8.3 (3H, OMe); −10.3 (1H, B-*H*); −21.0 (2H, *ortho*).

**$Tp^{Me,Me}$Ni-S-$C_6H_4$-4-$CH_3$ (7).** Anal. Calcd (found) for $C_{22}H_{29}BN_6NiS$: C, 55.16 (55.18); H, 6.10 (6.16); N 17.54

(13) Matsunaga, Y.; Fujisawa, K.; Ibi, N.; Miyashita, Y.; Okamoto, K.-i. *Inorg. Chem.* **2005**, *44*, 325–335.
(14) Cho, J.; Yap, G. P. A.; Riordan, C. G. *Inorg. Chem.* **2007**, *46*, 11308–11315.
(15) MacBeth, C. E.; Thomas, J. C.; Betley, T. A.; Peters, J. C. *Inorg. Chem.* **2004**, *43*, 4645–4662.
(16) Fox, D. C.; Fiedler, A. T.; Halfen, H. L.; Brunold, T. C.; Halfen, J. A. *J. Am. Chem. Soc.* **2004**, *126*, 7627–7638.
(17) Swenson, D.; Baenziger, N. C.; Coucouvanis, D. *J. Am. Chem. Soc.* **1978**, *100*, 1932–1934.
(18) Rosenfield, S. G.; Armstrong, W. H.; Mascharak, P. K. *Inorg. Chem.* **1986**, *25*, 3014–3018.
(19) Silver, A.; Koch, S. A.; Millar, M. *Inorg. Chim. Acta* **1993**, *205*, 9–14.
(20) Mueller, A.; Henkel, G. *Z. Naturforsch. B* **1995**, *50*, 1464–1468.
(21) Nguyen, T.; Panda, A.; Olmstead, M. M.; Richards, A. F.; Stender, M.; Brynda, M.; Power, P. P. *J. Am. Chem. Soc.* **2005**, *127*, 8545–8552.
(22) Evans, D. F.; Jakubovic, D. A. *J. Chem. Soc., Dalton Trans.* **1988**, 2927–2933.
(23) Santi, R.; Romano, A. M.; Sommazzi, A.; Grande, M.; Bianchini, C.; Mantovani, G. *J. Mol. Cat. A* **2005**, *229*, 191–197.
(24) Blower, P. J.; Dilworth, J. R.; Hutchinson, J. P.; Zubieta, J. A. *J. Chem. Soc., Dalton Trans.* **1985**, 1533–1541.
(25) Newton, A. *J. Am. Chem. Soc.* **1943**, *65*, 2439–2441.
(26) Bishop, P. T.; Dilworth, J. R.; Nicholson, T.; Zubieta, J. *J. Chem. Soc., Dalton Trans.* **1991**, 385–392.

(17.63). UV−vis ($CH_2Cl_2$, $\lambda_{max}$, nm; $\varepsilon$, $mM^{-1}$ $cm^{-1}$): 353 (1.7); 475 (2.4); 513 (3.2); 624 (sh, 0.2); 841 (0.1); 970 (sh, 0.1). $^1$H NMR ($CDCl_3$; $\delta$, ppm): 75.7 (3H, 4-pz); 38.1 (3H, *para-CH$_3$*); 23.1 (2H, *meta*); 6.4 (9H, 5-Me); −6.9 (9H, 3-Me); −10.4 (1H, B-*H*); −19.9 (2H, *ortho*).

**Tp$^{Me,Me}$Ni-S-C$_6$H$_4$-4-Cl (8).** Anal. Calcd (found) for $C_{21}H_{26}BClN_6NiS$: C, 50.50 (50.65); H, 5.25 (5.35); N 16.83 (16.70). UV−vis ($CH_2Cl_2$, $\lambda_{max}$, nm; $\varepsilon$, $mM^{-1}$ $cm^{-1}$): 361 (1.9); 464 (2.7); 510(2.8); 615 (sh, 0.2); 835 (0.2); 970 (sh, 0.1). $^1$H NMR ($CDCl_3$; $\delta$, ppm): 77.0 (3H, 4-pz); 23.7 (2H, *meta*); 7.1 (9H, 5-Me); −6.9 (9H, 3-Me); −10.5 (1H, B-*H*); −20.3 (2H, *ortho*).

**2.2. X-ray Crystallography.** The structure of Tp$^{Me,Me}$Ni-S-2,6-Ph$_2$C$_6$H$_3$·2.0THF (**5**) was solved at the University of Minnesota (VGY). Suitable crystals were grown from a concentrated THF solution cooled to −36 °C. An orange block (0.35 × 0.30 × 0.30 mm) was placed onto the tip of a 0.1 mm diameter glass capillary and mounted on a Bruker AXS diffractometer equipped with a CCD area detector.[27] The data collection was carried out at 123(2) K using Mo K$\alpha$ radiation ($\lambda$ = 0.71073 Å, graphite monochromator). The intensity data were corrected for absorption and decay (SADABS).[28] Final cell constants were calculated from 2761 strong reflections from the actual data collection after integration (SAINT).[29] The structure was solved and refined using Bruker SHELXTL.[30] The space group *Pnma* was determined based on systematic absences and intensity statistics. A direct-methods solution was calculated which provided most non-hydrogen atoms from the E-map; full-matrix least-squares difference Fourier cycles were performed which located the remaining non-hydrogen atoms. All non-hydrogen atoms were refined with anisotropic displacement parameters. All hydrogen atoms were placed in ideal positions and refined as riding atoms with relative isotropic displacement parameters. The molecule is bisected by the crystallographic mirror plane so that half appears in one asymmetric unit. There is also one molecule of THF solvent per asymmetric unit disordered over two positions in the same region of space in a 0.68:0.32 ratio. There is some indication that at least one THF fragment also has "envelope flap" disorder. It appears that the THF oxygen atoms were correctly placed for both disordered fragments. A total of 46783 reflections were collected, with 4718 being independent ($R_{int}$ = 0.0323) and 4062 observed. The refinement converged to give R1 = 0.0411, wR2 = 0.1042 (all data), GoF = 1.122. Crystal data: $C_{41}H_{51}BN_6NiO_2S_2$, formula weight 761.46, orthorhombic, *Pnma*, $a$ = 15.984(2) Å, $b$ = 23.499(3) Å, $c$ = 10.685(1) Å, $V$ = 4013.4(8) Å$^3$, Z = 4, $D_{calc}$ = 1.260 g/cm$^3$, $\mu$ = 5.78 cm$^{-1}$.

**2.3. DFT Calculations.** All calculations were carried out using the Amsterdam Density Functional software package (version 2007.01, Scientific Computing and Modeling NV).[31,32] Atomic coordinates were imported from the experimental structures of **1** and **5** and reduced to simple TpNi-SPh models **1′** and **5′** by replacement of the pyrazole and *ortho*-arylthiolate substituents with hydrogen atoms in ideal positions. The model geometries were optimized under imposed $C_s$ symmetry, with the Ni−S−C$_{ipso}$ angle of **5′** constrained to the experimental value to prevent inward bending in the absence of the 3-pyrazole and ortho-arylthiolate substituents. Furthermore, a full series of configurational models spanning arylthiolate coordination with equatorial or axial sulfur ligation and horizontal or vertical substituent orientations was obtained by manipulating the N$_{axial}$−Ni−S-C$_{ipso}$ and Ni−S−C$_{ipso}$-C$_{ortho}$ torsion angles of **5′** with subsequent geometry optimization under appropriate symmetry (i.e., $C_1$ or $C_s$) without additional constraints. Finally, a **1″** model optimized under experimental $C_1$ symmetry was also included in TD-DFT calculations. Spin-unrestricted geometry optimizations, single point and TD-DFT[33,34] calculations were performed using the Vosko−Wilk−Nussair LDA exchange-correlation functional,[35] the Becke−Perdew GGA correction,[36,37] and the Slater-type orbital TZP (triple-$\zeta$ with single polarization) basis set available in the ADF library, with frozen atomic cores and default convergence criteria. A solvation model and relativistic correction were not applied. Spin-restricted calculations on the free phenylthiolate anion were performed similarly, starting from a suitable crystal structure fragment.

## 3. Results and Discussion

**3.1. General Comments.** We prepared several derivatives of Tp$^{Me,Me}$Ni-SPh (**1**), our previously reported parent complex,[9] modified along steric and electronic vectors: a series of complexes with enhanced bulk at the *ortho* arylthiolate positions, Tp$^{Me,Me}$Ni-SAr [Ar = C$_6$H$_5$ (**1**), 2,6-Me$_2$-C$_6$H$_3$ (**2**), 2,4,6-Me$_3$-C$_6$H$_2$ (**3**), 2,4,6-$^i$Pr$_3$-C$_6$H$_2$ (**4**), 2,6-Ph$_2$-C$_6$H$_3$ (**5**)]; and a second series with *para* substituents, Tp$^{Me,Me}$Ni-S-C$_6$H$_4$-4-X [X = OCH$_3$ (**6**), CH$_3$ (**7**), H (**1**), and Cl (**8**)], of varying electronic donor strength. The complexes were prepared from Tp$^{Me,Me}$NiCl by metatheses with respective sodium thiolate salts in THF, resulting in appearance of intense coloration due to characteristic Ni-SAr LMCT bands (vide infra). The complexes were characterized by elemental analyses, $^1$H NMR and UV−vis-NIR spectroscopy. In all cases, the results were consistent with pseudotetrahedral complexes exhibiting a paramagnetic ($S$ = 1) d$^8$ electron configuration. The structure of **5** was also determined.

**3.2. X-ray Crystallography.** The previously reported structures of Tp$^{Me,Me}$NiSPh (**1**) and the bulkier analogue Tp$^{Ph,Me}$Ni-S-2,6-Me$_2$C$_6$H$_3$ (**9**) consisted of distorted pseudotetrahedral N$_3$S ligand fields with the Ni−S bond tilted off the 3-fold H−B···Ni axis particularly toward one of the pyrazolyl arms, giving a trigonal pyramidal shape with an N$_2$S equatorial plane.[9] The arylthiolate substituents were disposed over unoccupied axial sites and nearly vertical between 3-pyrazole substituents on opposing equatorial donor arms. In the present work, we introduced steric bulk at the arylthiolate *ortho* positions while retaining the smaller 3-pyrazole methyl substituents. This elicited a distinct arylthiolate coordination mode, revealed by the crystal structure of Tp$^{Me,Me}$-Ni-S-2,6-Ph$_2$C$_6$H$_3$ (**5**), which is distorted by off-axis thiolate bending toward a sawhorse geometry, with axial sulfur and pyrazole donors (i.e., S1 and N2) and an open equatorial site (Figure 1). The Ni−S bond in **5** is bent between pyrazole donors, and the arylthiolate substituent is displaced backward over the third pyrazole and the

(27) *SMART*, V5.054; Bruker Analytical X-ray Systems: Madison, WI, 2001.
(28) An empirical correction for absorption anisotropy: Blessing, R. *Acta Crystallogr.* **1995**, *A51*, 33–38.
(29) *SAINT+*, V6.45; Bruker Analytical X-Ray Systems: Madison, WI, 2003.
(30) *SHELXTL*, V6.14; Bruker Analytical X-Ray Systems: Madison, WI, 2000.
(31) *ADF 2007.01, Scientific Computing and Modelling NV*; Vrije Universiteit: Amsterdam, The Netherlands, 2007.
(32) te Velde, G.; Bickelhaupt, F. M.; Baerends, E. J.; Fonseca Guerra, C.; van Gisbergen, S. J. A.; Snijders, J. G.; Ziegler, T. *J. Comput. Chem.* **2001**, *22*, 931–967.
(33) van Gisbergen, S. J. A.; Snijders, J. G.; Baerends, E. J. *Comput. Phys. Commun.* **1999**, *118*, 119–138.
(34) Wang, F.; Ziegler, T. *Mol. Phys.* **2004**, *102*, 2585–2595.
(35) Vosko, S. H.; Wilk, L.; Nusair, M. *Can. J. Phys.* **1980**, *58*, 1200–1211.
(36) Becke, A. *Phys. Rev.* **1988**, *A38*, 3098–3100.
(37) Perdew, J. P. *Phys. Rev.* **1986**, *B33*, 8822–8824.

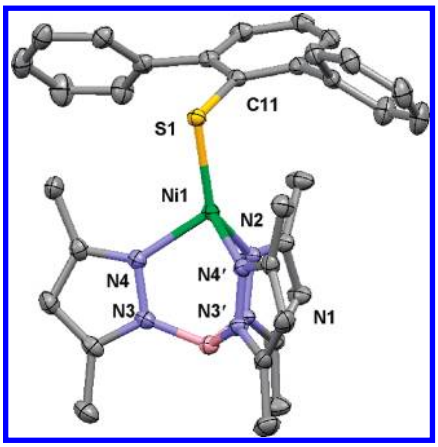


**Figure 1.** ORTEP diagram (50% ellipsoids) of $Tp^{Me,Me}$Ni-S-2,6-$Ph_2C_6H_3$ (**5**). Selected bond lengths (Å): Ni1−N4, 1.995(1); Ni1−N2, 2.001(2); Ni1−S1, 2.2589(6); S1−C11, 1.785(2). Bond angles (deg): N4−Ni1−N4′, 92.06(8); N4−Ni1−N2, 91.20(5); N4−Ni1−S1, 115.47(4); N2−Ni1−S1, 140.01(6); Ni1−S1−C11, 100.11(7).

vacant equatorial site, rotating into a rigorously horizontal orientation (molecular $C_s$ symmetry is enforced by a crystallographic mirror plane). The outer 2,6-phenyl ring planes are rotated 55.89° from coplanarity, giving short contacts between each of the pyrazole 3-methyl substituents and an opposing aromatic ring on the arylthiolate, 3.330 and 3.503 Å to the inner and outer centroids, respectively. The unique N−Ni−S angle from the axial pyrazole increases from 113.26(6)° in **1** to 140.01(6)° in **5**, with further opening possibly constrained by the equatorial 3-methyl substituents, given short S···HC contacts of 2.883 Å. The Ni−S bond length is slightly longer in **5** than in **1**, 2.2589(6) versus 2.216(1) Å, while the Ni−S−Ar angle is less obtuse, 100.11(7) versus 103.84(8)°.

**3.3. Ni-SAr Structural Configurations.** Tris(pyrazolyl)borates and related tripodal ligands have been referred to as "tetrahedral enforcers" for the four-coordinate, half-sandwich geometry they support.[38−40] However, the tetrahedral ligand fields are typically distorted (hence "pseudotetrahedral"), and several unique distortional modes have been identified by symmetry mapping of four-coordinate metal centers.[41] A universal $T_d \rightarrow C_{3v}$ umbrella distortion is enforced by the constrained ligand bite, in which N−Ni−N angles are reduced to about 90°, and the angle to the trigonal H−B···Ni axis is concordantly increased to about 124° for the tris(pyrazolyl)borate ligand. Such facially tridentate ligands are perhaps more appropriately assigned as filling one face of an octahedron, particularly when an apical co-ligand can donate six electrons utilizing orthogonal lone pairs of $\pi$ symmetry, such as CO or halide anions.[38−40] The borate chelate also constrains $T_d \rightarrow D_{2d}$ spread and plier distortions, the former having been observed for $[Ni(SAr_4)]^{2-}$ complexes,[17−20] but the apical arylthiolate ligand is still susceptible to $T_d \rightarrow C_s$ off-axis and $T_d \rightarrow C_{2v}$ sawhorse bendings.[41] With three positions defined by constrained facial pyrazolyl nitrogens, the off-axis and sawhorse bendings are limited to opposing motions of the sulfur toward or away from a particular pyrazole ring. These will respectively lead to a unique N−Ni−S angle that is smaller or larger than the average umbrella angle.

Relevant geometric parameters for the seven structurally characterized arylthiolate complexes of Ni(II) supported by tripodal borate ligands can be summarized within this model (Table 1).[9,13−15] A significant umbrella distortion is indicated in each case by the pseudotetrahedral angle formed between the 3-fold H−B···Ni axis and the coordinate bond vectors to the borate tripod donor atoms (L) ranging from 120.4° to 124.8° compared to the ideal tetrahedral value of 109.47°. Further distortion by off-axis or sawhorse bending of the arylthiolate is indicated by distribution of L−Ni−S angles about this value. As predicted in limiting cases, one of the three L−Ni−S angles is unique, being smaller (e.g., **9**) or larger (e.g., **5**) than the pseudotetrahedral angle.

The sawhorse distortion has been structurally analyzed in terms of a *cis*-divacant octahedron (Figure 2, left),[39,40] in which Ni−S bending toward an edge of the $L_3$ donor triangle leads to a staggered geometry, illustrated for the core structure of **5** (Figure 2, top). Off-axis bending can be interpreted in the opposite direction, toward a vertex that yields an eclipsed geometry typified by **9** (Figure 2, bottom). Since a *bent* arylthiolate ligand can donate only four electrons, these distortions can be alternatively considered on the surface of a monovacant trigonal bipyramid (Figure 2, right),[13,14,38,42] overlooking the constrained bite of the equatorial nitrogens. Nevertheless, bending of sulfur toward distinct axial or equatorial sites gives the same two limiting geometries. The Ni−S bond is bent directly over a donor in the trigonal/eclipsed/equatorial geometry, and directly away in the sawhorse/staggered/axial geometry. Equivalence of the octahedral and trigonal bipyramidal models can be observed by rotation of the corresponding core structures of **5** and **9** about the axial pyrazole nitrogen. The trigonal bipyramidal nomenclature (i.e., axial and equatorial) seems the most descriptive of the ligand field and will be used exclusively henceforth, with "axial" coordination denoting distortion toward a trigonal bipyramidal vertex as opposed to a site along the H−B···Ni umbrella axis.

The limiting axial and equatorial configurations just defined are further differentiated by orthogonal orientations of the aryl substituent (Figure 2). The substituent is usually folded backward over the vacated site and rotated to minimize steric contact with the opposing tripodal ligand substituents. The axial thiolate configurations of **5** and the $PhBP_3$Ni-S-$C_6H_4$-4-$^t$Bu complex reported by MacBeth, et al.[15] are associated with a "horizontal" disposition of the aryl substituent, denoted by large Ni−S−$C_{ipso}$−$C_{ortho}$ torsion angles (Table 1), while an equatorial, vertical orientation is observed in the other structures.

The magnitudes of distortions of tetracoordinate complexes from tetrahedral toward a trigonal monopyramid have been quantified either by a $\tau$ parameter ranging from zero to unity, based on the difference of apical and basal bond angles,[42] or inversely by metal separation from an

(38) Jenkins, D. M.; Peters, J. C. *J. Am. Chem. Soc.* **2005**, *127*, 7148–7165.
(39) Kersten, J. L.; Kucharczyk, R. R.; Yap, G. P. A.; Rheingold, A. L.; Theopold, K. H. *Eur. J. Chem.* **1997**, *3*, 1668–1674.
(40) Detrich, J. L.; Konečný, R.; Vetter, W. M.; Doren, D.; Rheingold, A. L.; Theopold, K. H. *J. Am. Chem. Soc.* **1996**, *118*, 1703–1712.
(41) Cirera, J.; Alemany, P.; Alvarez, S. *Eur. J. Chem.* **2004**, *10*, 190–207.
(42) Vela, J.; Stoian, S.; Flaschenriem, C. J.; Münck, E.; Holland, P. L. *J. Am. Chem. Soc.* **2004**, *126*, 4522–4523.

**Table 1.** Structural Parameters for Ni(II) Arylthiolate Complexes of Tripodal Borato Ligands

| complex | umbrella angle (deg)[a] | L−Ni−S angles (deg) | Ni−S−$C_{ipso}$−$C_{ortho}$ torsion angles (deg) | $d$ (Å)[b] | $\tau$[c] | $\tau_4$[d] | ref. |
|---|---|---|---|---|---|---|---|
| $Tp^{Ph,Me}$Ni-S-2,6-$Me_2C_6H_3$ (**9**) | 124.8 | 135.73(5), 129.95(5), 103.05(5) | 15.14, 15.19 | 0.20 | 0.81 | 0.67 | 9 |
| $PhTt^{tBu}$Ni-$SC_6F_5$[e] | 122.9 | 130.29(2), 128.52(2), 105.13(2) | 5.35, 7.15 | 0.28 | 0.74 | 0.70 | 14 |
| $Tp^{iPr,iPr}$Ni-$SC_6F_5$[f] | 124.0 | 132.7(1), 128.9(1), 106.8(1) | 10.41, 11.62 | 0.28 | 0.72 | 0.70 | 13 |
| | 123.8 | 132.8(1), 128.4(1), 106.4(1) | 10.84, 11.90 | | | | |
| $PhTt^{tBu}$Ni-SPh[e] | 122.3 | 129.94(4), 129.00(4), 104.49(4) | 1.03, 1.66 | 0.31 | 0.69 | 0.72 | 14 |
| $Tp^{Me,Me}$Ni-SPh (**1**) | 124.0 | 134.96(6), 122.69(6), 113.26(6) | 16.11, 16.64 | 0.37 | 0.60 | 0.73 | 9 |
| $Tp^{Me,Me}$Ni-S-2,6-$Ph_2C_6H_3$ (**5**) | 124.2 | 140.01(6), 115.47(4), 115.47(4) | 89.46, 89.46 | 0.42 | g | 0.74 | h |
| $PhBP_3$Ni-S-$C_6H_4$-4-$^t$Bu[i] | 120.4 | 151.84(3), 109.79(3), 101.54(3) | 67.32, 68.66 | 0.32 | g | 0.70 | 15 |

[a] The average umbrella angle between the 3-fold H−B···Ni axis and the L−Ni bond vectors (i.e., 109.47° for $T_d$ symmetry). [b] Displacement of Ni from an equatorial $L_2S$ plane, see ref 13. [c] [Σ∠(basal-basal) − Σ∠(apical−basal)]/90, see ref 42. [d] (360° − α − $\beta$)/141°, where α and $\beta$ are the two largest interligand angles, see ref 43. [e] $PhTt^{tBu}$ = phenyltris(tert-butylthiomethyl)borate, $[PhB(CH_2S^tBu)_3]^-$. [f] Two independent molecules. [g] Undefined. [h] This work. [i] $PhBP_3$ = phenyltris(diphenylphosphinomethyl)borate, $[PhB(CH_2PPh_2)_3]^-$.

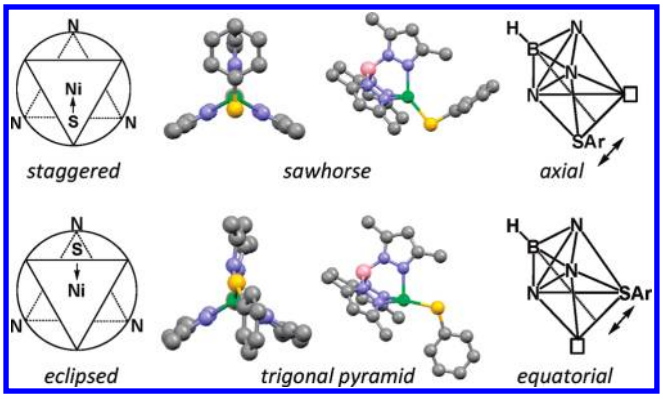


**Figure 2.** Illustration of sawhorse (top) and off-axis bending (bottom) on a *cis*-divacant octahedron (left column) and monovacant trigonal bipyramid (right column), as seen in two orientations of the core structures for **5** (top row) and **9** (bottom row), with *ortho* substituents on the arylthiolate rings and all but the *ipso* carbon of the 3-phenyl substituents of **9** omitted for clarity.

equatorial $N_2S$ basal plane.[13] A uniquely large N−Ni−S angle consistent with a sawhorse geometry gives an undefined $\tau$ value. However, a different $\tau_4$ parameter defined by the two largest bond angles encompasses both distortions, such that unity corresponds to a tetrahedron (reduced to 0.78−0.85 by the umbrella distortion), while a sawhorse and a trigonal pyramid are independently defined as 0.64 (with 90° N−Ni−N angles).[43] These various parameters are also summarized for each tripodal arylthiolate complex (Table 1).

As discussed previously, the off-axis and sawhorse bendings are energetically favored for a $d^8$ electron configuration by reduction of destabilizing overlap in the filled Ni−S d$\sigma$-p$\sigma$* interaction.[40] While electronic in origin, the direction and magnitude of the bending can be manipulated by steric contacts. We previously demonstrated enhanced trigonal bending from **1** to **9** ($\tau$ = 0.60 and 0.81, respectively, Table 1) by substituting bulky 3-pyrazole substituents (i.e., $Tp^{Ph,Me}$) proximal to added *ortho*-methyl substituents on the arylthiolate ring.[9] The rigid 3-phenyl rings enforced retention of a vertical 2,6-xylyl substituent orientation in **9**, leaving the sulfur in an equatorial configuration with enhanced off-axis bending. With retention of the smaller $Tp^{Me,Me}$ ligand substituents, rotation of the arylthiolate ring is enabled, and the bulky thiolate of **5** adopts an axial/horizontal configuration. We hypothesize that the equatorial/vertical configuration lies somewhat lower in energy for **1**, but is destabilized by enhanced steric contact with ortho-phenyl substituents in **5**, thus effecting a conformational switch (Figure 3). This suggests a dynamic equilibrium between the configurations can be manipulated by changing the size of added *ortho* arylthiolate substituents. Spectroscopic evidence supporting this interpretation was obtained across the series **1**−**5** encompassing added 2,6-$Me_2$, -$^i$Pr$_2$, and -$Ph_2$ arylthiolate disubstitution of **1**.

**3.4. $^1$H NMR Spectroscopy.** NMR spectra obtained for paramagnetic complexes **1**−**8** were consistent with their formulations, notwithstanding significant paramagnetic shifts induced by unpaired electrons ($S$ = 1) on high-spin Ni(II). A prominent feature common to all the spectra was a single resonance for three equivalent 4-pyrazole protons with a pronounced downfield shift (Figure 4). Equivalent 3- and 5-methyl resonances were also observed much closer to the diamagnetic region, with the former significantly broadened by the proximal paramagnet. A borohydride resonance and additional signals consistent with the various aryl substituents were also observed. Compared to the static crystal structures, equivalence of all three pyrazoles and both arylthiolate faces is indicative of rapid migration of the arylthiolate on the NMR time scale, minimally between equivalent binding sites about the 3-fold H−B···Ni axis.

The alternating upfield and downfield shifts for the arylthiolate protons of **1**, as well as reversal of *ortho* and *para* polarization with methyl substitution in **3**, are consistent with hyperfine contact shifting because of electron spin delocalization onto the arylthiolate by a $\pi$-polarization pathway.[9] The *para* protons of **2** and **5** exhibit a striking attenuation of upfield shift, consistent with quenching of the $\pi$-polarization upon orthogonal rotation of the aryl substituent evident between the crystal structures of **1** and **5**. Thus, the solid state structures of **1** and **5** are plausibly maintained as predominant conformations in solution, with **2** partitioning in a dynamic equilibrium between these two limits. The 3-pyrazole methyl protons also exhibited a much smaller monotonic increase in upfield shift with increasing steric bulk of **1**−**5**, which may represent differential diamagnetic shifts arising from aromatic ring currents on the proximal thiolate, consistent with the proposed conformation change. In contrast, the *meta* protons of **1**−**5** maintain a nearly

(43) Yang, L.; Powell, D. R.; Houser, R. P. *Dalton Trans.* **2007**, 955–964.

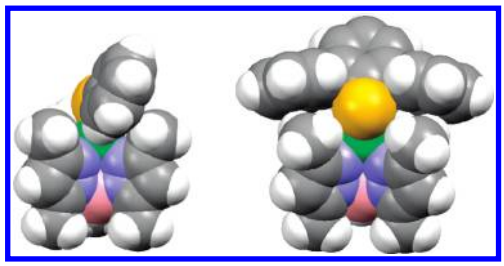

**Figure 3.** Space-filling models of **1** (left) and **5** (right), demonstrating a dominant steric role for *ortho* substitution in effecting an observed conformational switch in arylthiolate coordination.

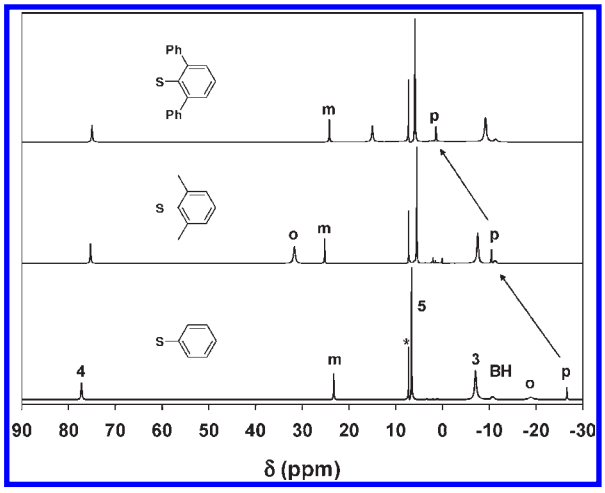


**Figure 4.** $^1$H NMR spectra of **1**, **2**, and **5** (from bottom to top, respectively) recorded in $CDCl_3$ at 295 K. The peak marked (*) is residual solvent; peak assignments not labeled are listed in the experimental section. Arrows indicate shift of the resonance assigned to the *para* position of the arylthiolate rings.

constant downfield shift, indicative of a second mechanism, such as direct spin delocalization through $\sigma$ bonds. J-coupling between the assigned *meta* and *para* protons of **2** and **5** were established by COSY techniques (see Supporting Information).

The series of *para*-substituted arylthiolate complexes **6**−**8** was also examined. Not surprisingly, $^1$H NMR spectra were nearly identical to that of **1**, absent the upfield *para* proton resonance and addition of either a broad upfield methoxy resonance in **6** or a downfield methyl resonance in **7**. The remaining resonances exhibited comparable chemical shifts to those of **1**, except for a slight upfield shift of the 4-pyrazole protons in **6** and **7**. These observations demonstrate the absence of significant electronic effects on Ni−S bonding, with the structure of **1** retained over the series **6**−**8**.

**3.5. Electronic Spectroscopy.** The previously reported UV−vis-NIR spectrum of **1** in $CH_2Cl_2$ revealed multiple transitions, with three strong bands (354, 464, and 506 nm) apparently exhibiting S−Ni LMCT character.[9] The three spin-allowed ligand field transitions of a tetrahedral $d^8$ metal ion were split by the effective $C_s$ symmetry, yielding several relatively weak and broad bands at lower energy (614, 836, 970, and 1580 nm) and

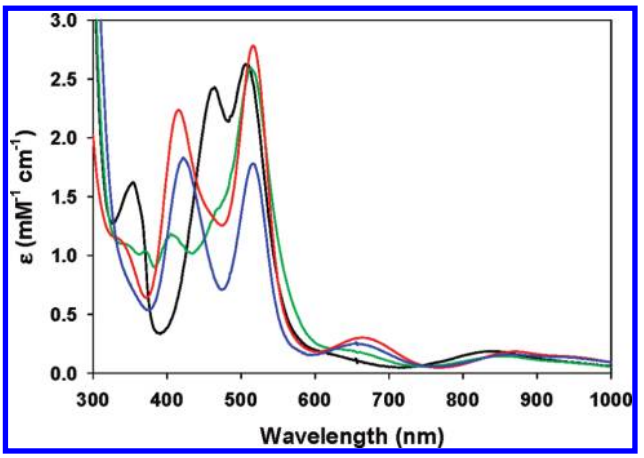


**Figure 5.** UV−visible−NIR spectra ($CH_2Cl_2$ solutions, 297 K) of **1** (black), **3** (green), **4** (red), and **5** (blue).

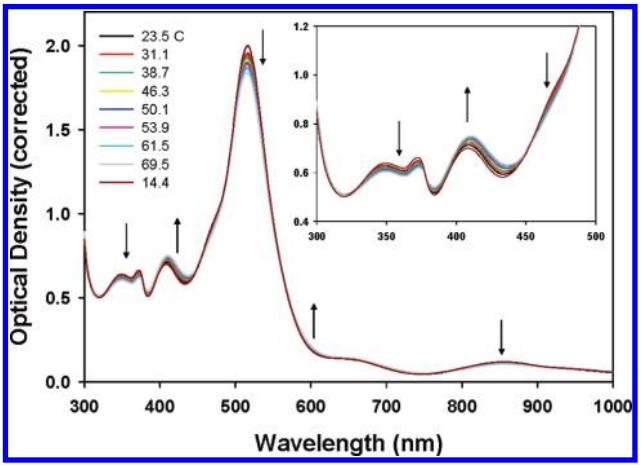


**Figure 6.** UV−visible−NIR spectra of **3** in toluene as a function of temperature from 287 to 343 K. Spectra were normalized for changes in solvent density.[46] Raw data are shown in Supporting Information.

obfuscating more precise assignment. Analysis of absorption and MCD spectra for $Tp^{iPr,iPr}Ni$-$SC_6F_5$ in cyclohexane yielded qualitatively similar assignments,[44] and comparable ligand field bands under $C_{3v}$ symmetry were also reported for $Tp^{Me,Me}NiCl$ in $CH_2Cl_2$.[45]

Compared to **1**, the *ortho*-disubstituted arylthiolate complexes **3**−**5** yielded dramatically different UV−vis spectra (Figure 5). The 506 nm CT band was retained, but the 464 and 354 nm bands seemed to progressively collapse in **3**−**5**, while a new feature appeared at intermediate wavelengths. The ligand field bands also shifted dramatically, with emergence of a broad band near 660 nm. Taken together, the overlaid spectra give the appearance of a titration plot, presumably representing distributions of the two distinct conformations already elucidated. Complexes **1** and **5** would retain the respective equatorial/vertical and axial/horizontal configurations defined in the solid state, while **3** and **4** with intermediate steric bulk would partition between these configurations. Of course, the features of **3**−**5** would display minor differences in energy and extinction because of chemical modification

(44) Gorelsky, S. I.; Basumallick, L.; Vura-Weis, J.; Sarangi, R.; Hodgson, K. O.; Hedman, B.; Fujisawa, K.; Solomon, E. I. *Inorg. Chem.* **2005**, *44*, 4947–4960.

(45) Desrochers, P. J.; Telser, J.; Zvyagin, S. A.; Ozarowski, A.; Krzystek, J.; Vicic, D. A. *Inorg. Chem.* **2006**, *45*, 8930–8941.

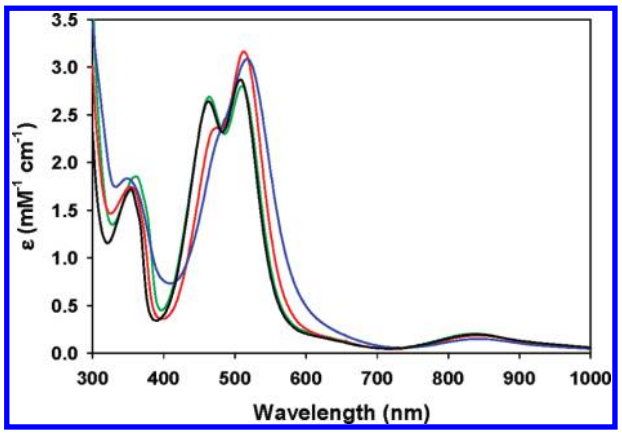


**Figure 7.** UV−visible−NIR spectra ($CH_2Cl_2$ solutions, 297 K) of **1** (black), **6** (blue), **7** (red), and **8** (green).

of the arylthiolate, and legitimate isosbestic points are not observed.

To test this hypothesis, spectra of the mesityl complex **3** were recorded in toluene over a temperature range of 287−343 K (Figure 6). Fully reversible temperature-dependent absorption changes were observed with at least four isosbestic points, consistent with perturbation of a two-state equilibrium. In particular, a CT feature at 412 nm emerged with increasing temperature at the expense of flanking bands, analogous to the preceding comparison of **1** and **5** (Figure 5). The spectral features of **3** show surprisingly little difference between $CH_2Cl_2$ and toluene solutions despite a significant change in solvent polarity.

To further probe the charge transfer features of **1**, spectra were obtained for the series of *para*-substituted arylthiolate complexes $Tp^{Me,Me}$Ni-S-$C_6H_4$-*p*-X (X = OMe, **6**; Me, **7**; H, **1**; and Cl, **8**, Figure 7). All four spectra yielded similar ligand field bands, exhibiting only a slight red-shift in the order **8** < **1** < **7** < **6**, paralleling the overall donor strength of the arylthiolates. This result is again indicative of a common solution structure. In contrast, the strong charge transfer features at 464 and 506 nm were more noticeably red-shifted, with the former band showing a larger effect, in the order **1** < **8** < **7** < **6**, following relative $\pi$-donor strengths consistent with S−Ni p$\pi$-d$\pi$* LMCT character. Finally, the weaker CT band at 354 nm displayed a reversed red-shift pattern, **6** < **7** < **1** < **8**, with retention of the poorly resolved fine structure. The contrasting behaviors of the three strong CT bands indicate complexity in the nickel-arylthiolate bonding interaction.

**3.6. DFT Calculations.** To further rationalize the divergent arylthiolate configurations and spectroscopic results observed for **1** and **5**, spin-unrestricted DFT calculations were performed on simplified TpNiSPh computational models **1′** and **5′** constructed from the respective crystal structures by substitution of hydrogen atoms for pyrazole and arylthiolate substituents and geometry optimization under imposed $C_s$ symmetry. Orbital energies and allowed electronic transitions were calculated for both models. Of principal interest in Ni-SAr bonding are eight $\beta$-spin frontier orbitals corresponding to the five d orbitals split by the ligand field and three arylthiolate

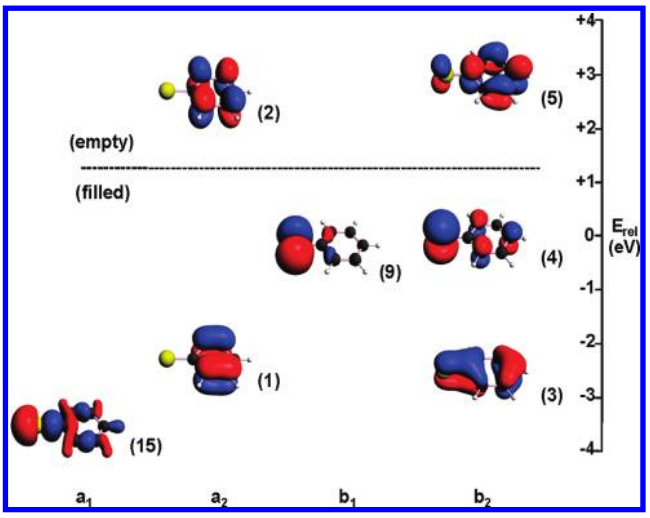


**Figure 8.** Relevant frontier orbitals of the free $PhS^-$ ligand, separated by symmetry class. The dashed horizontal line separates occupied and empty orbitals.

donor orbitals. The metal and thiolate fragments are first discussed separately, and then together as Ni-SR complexes. An expanded range of limiting arylthiolate configurations incorporating **1′** and **5′** was defined on the basis of Ni-SAr bending and scaled by calculated relative energies, and TD-DFT calculations were performed to assign CT features in electronic spectra.

**3.6.1. Arylthiolate Donor Orbitals.** Spin-restricted calculations were performed for the free $C_6H_4S^-$ anion after geometry optimization under $C_{2v}$ symmetry (Figure 8). Of the three sulfur 3p orbitals available for bonding with nickel, one is coincident with the S−$C_{ipso}$ bond vector and significantly stabilized ($15a_1$). The other two comprise nearly degenerate lone pairs at high energy (i.e., HOMO and HOMO-1), one coplanar with the phenyl ring ($9b_1$, 93% S), and the other perpendicular to the ring and delocalized onto it. The symmetry and intermediate energy of the latter atomic orbital with respect to the one- and two-node Hückel $\pi$ orbitals on the substituent ring result in bonding ($3b_2$, 16% S), non-bonding ($4b_2$, 69% S), and antibonding ($5b_2$, 13% S) combinations. The $4b_2$ HOMO is destabilized by only 0.07 eV relative to $9b_1$. These two donor orbitals have been referred to respectively as $\pi_{op}$ and $\pi_{ip}$ in previous work,[15,21,47,48] although one of these must adopt a pseudo-$\sigma$ orientation for a bent thiolate,[44] depending on the configurational geometry. The $3b_2$ orbital is stabilized by 2.06 eV compared to the $4b_2$ HOMO, and by 0.37 eV relative to its symmetry-isolated Hückel congener ($1a_2$). Despite this stabilization and consequent attenuation of S 3p contribution, the $3b_2$ orbital exhibits the same symmetry as $\pi_{op}$, and subsequent calculations on the arylthiolate complexes suggest a role for this third donor orbital in differentiating the bonding and spectroscopy of the two arylthiolate conformations of **1** and **5** (vide infra).

**3.6.2. Nickel Acceptor d Orbitals.** Ligand field splitting of d orbitals for a pseudotetrahedral Ni(II) ion can be

(46) Kashiwagi, H.; Hashimoto, T.; Tanaka, Y.; Kubota, H.; Makita, T. *Int. J. Thermophysics* **1982**, *3*, 201–215.

(47) Davis, M. I.; Orville, A. M.; Neese, F.; Zaleski, J. M.; Lipscomb, J. D.; Solomon, E. I. *J. Am. Chem. Soc.* **2002**, *124*, 602–614.

(48) Ghosh, S.; Cirera, J.; Vance, M. A.; Ono, T.; Fujisawa, K.; Solomon, E. I. *J. Am. Chem. Soc.* **2008**, *130*, 16262–16273.

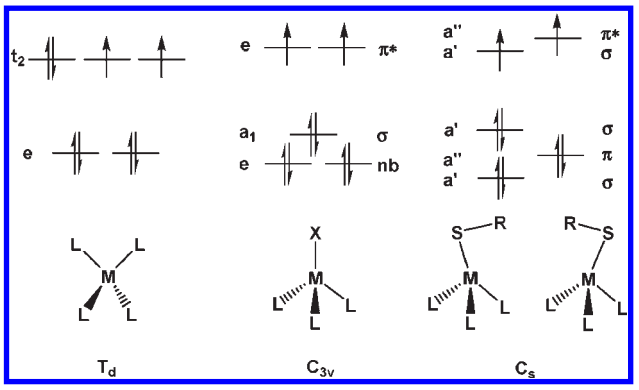


**Figure 9.** Qualitative symmetry-derived ligand field splittings for tetrahedral (left), axial pseudotetrahedral (center), and bent arylthiolate geometries (right).

qualitatively anticipated by symmetry reduction from $T_d$, with upper $t_2$ ($d_{xy}$, $d_{xz}$, $d_{yz}$) and lower e ($d_{x^2-y^2}$, and $d_{z^2}$) sets (Figure 9, left). Umbrella distortion yields $C_{3v}$ symmetry with reduced N−Ni−N angles, causing axial destabilization that is offset in the perpendicular equatorial plane. This gives rise to an axial $d_{z^2}$ orbital sandwiched between e sets ($d_{xz}$,$d_{yz}$ over $d_{xy}$,$d_{x^2-y^2}$; Figure 9, center).[45] The former exhibit $\pi$ symmetry toward the axial ligand, while the filled $d_{z^2}$ orbital assumes $\sigma$ symmetry, and the equatorial $d_{xy}$,$d_{x^2-y^2}$ pair is non-bonding.[15,45] Off-axis or sawhorse bending further reduces symmetry to $C_s$, breaking the equatorial degeneracy. The e orbital pairs are slightly split; within each pair, one orbital adopts $\sigma$ symmetry while the other exhibits $\pi$ overlap (Figure 6, right). Consequent elaboration of $\sigma$ interactions stabilizes the distortion. The standard setting of the $C_s$ point group invokes an $x$,$y$ mirror plane containing the nickel−sulfur bond. The $d_{xy}$, $d_{x^2-y^2}$, and $d_{z^2}$ orbitals are symmetric under reflection and encompass Ni-SPh $\sigma$ bonding under a′ symmetry, while antisymmetric $d_{xz}$, $d_{yz}$ orbitals are $\pi$ bonding under a″ symmetry.

**3.6.3. Ni-SAr Bonding.** Spin unrestricted calculations were performed on TpNiSPh models **1**′ and **5**′ under enforced $C_s$ symmetry, focusing on eight $\beta$-spin molecular orbitals corresponding to the five nickel d orbitals and three arylthiolate donor orbitals. These are illustrated for both models (Figure 10). Bonding in **1**′ and **5**′ were considered in detail to elucidate the differences between the diametrically opposed equatorial/vertical and axial/horizontal configurations. Previous calculations on TpNi-$SC_6F_5$ in the equatorial/vertical coordination mode analogous to **1**′ assigned thiolate $\pi_{ip}$ and $\pi_{op}$ donor orbitals intermediate energies with respect to the d orbital manifold; the $\pi_{op}$ orbital was stabilized by a p$\pi$-d$\pi$* interaction with a half-filled Ni d orbital, while the perpendicular $\pi_{ip}$ orbital was destabilized by a filled−filled interaction of pseudo-$\sigma$ symmetry.[44] A qualitatively similar electronic structure was found for **1**′ (Figure 10, left), with the arylthiolate $\pi_{op}$ and $\pi_{ip}$ donor orbitals (21a″ and 40a′, respectively) retaining analogous bonding roles. In the axial/horizontal configuration of **5**′, these donor orbitals (24a″ and 37a′) necessarily exchange their roles because of orthogonal rotation of the arylthiolate substituent, and bonding overlap is altered by displacement of the sulfur atom within the ligand field. These combined symmetry effects must be the root cause of the spectroscopic differences between **1** and **5** in their distinctive configurations. The two highest molecular orbitals (i.e., 41a′ and 22a″ in **1**′ and 38a′ and 25a″ in **5**′) are primarily nickel-centered d orbitals destabilized by strong Ni−N $\sigma$* interactions, and are unoccupied, consistent with a $d^8$ electron count for Ni(II) and a paramagnetic, $S = 1$ ground state in both complexes.

Three $\beta$-spin frontier orbitals exhibit Ni−S $\pi$-bonding symmetry in the axial/horizontal thiolate coordination of **5**′ (23a″-25a″; Figure 10, right). The highest orbital is unoccupied and metal-centered (25a″: 59% Ni $d_{yz}$; 19% S $p_z$), representing Ni−S d$\pi$-p$\pi$* character. The intermediate orbital represents the $\pi_{ip}$ orbital with a minor non-bonding metal contribution (24a″: 22% Ni $d_{xz}$, 15% $d_{yz}$; 47% S $p_z$). The lowest orbital is a metal centered $\pi$-bond (23a″: 41% Ni $d_{xz}$; 22% S $p_z$). Overlap in this orbital is favorably directed toward the axial sulfur, but minimized in the empty 25a″ antibonding orbital that is directed toward the vacant equatorial site. Significant Ni−S $\pi$ covalency is therefore indicated.

The five other relevant $\beta$-spin orbitals of **5**′ (32a′ and 35a′-38a′) exhibit a′ symmetry appropriate for Ni−S $\sigma$ bonding. Two of the orbitals are primarily metal-centered (36a′: 39% $d_{z^2}$, 31% $d_{x^2-y^2}$; 38a′: 44% $d_{x^2-y^2}$, 21% $d_{z^2}$) and present nodal planes toward the sulfur atom, rendering them essentially non-bonding (< 4% S $p_x$). Similar to 25a″, the latter is destabilized by a Ni−N $\sigma$* interaction and is unoccupied. The third d orbital (35a′: 39% $d_{xy}$, 12% $d_{z^2}$) is properly aligned to overlap with the $\pi_{op}$ orbital (37a′: 33% $d_{xy}$; 28% S $p_x$). However, this orbital is lacking any sulfur contribution (ca. 1% S $p_x$), despite obvious delocalization onto the aryl substituent. The third arylthiolate donor orbital, specifically the one-node Hückel donor orbital $3b_2$ (32a′: 13% $d_{xy}$; 33% S $p_x$), brackets the d manifold from below, and with the $\pi_{op}$ donor orbital above, forms a stack of three $\sigma$ orbitals with bonding, non-bonding, and antibonding character. The $\sigma$ bonding can be described as a three-center interaction between nickel, sulfur, and the aryl substituent. The intermediate non-bonding orbital (35a′) exhibits significant Ni d character and a node on the central sulfur atom, while the bonding orbital (32a′) is fully delocalized and stabilized by an additional 0.8 eV below the symmetry-isolated one-node Hückel congener (21a′, not shown in Figure 10; cf., $1a_2$ in Figure 8). As all three orbitals are filled, net Ni−S d$\sigma$-p$\sigma$* bonding is not obtained.

The difference in arylthiolate coordination in **1**′ compared to **5**′ is displacement of sulfur from an axial to an equatorial position, with a concordant back-flip and orthogonal rotation of the aryl substituent from horizontal to vertical. This perturbs several aspects of Ni-SAr bonding elucidated for **5**′ (Figure 10, left). Aryl substituent rotation swaps the pseudo-$\sigma$ and $\pi$ bonding roles of the thiolate $\pi_{op}$ and $\pi_{ip}$ donor orbitals (21a″ and 40a′ in **1**′, respectively); the third thiolate $3b_2$ donor orbital is also transformed from $\sigma$ to $\pi$ symmetry in **1**′ (14a″), stabilizing the overall $\sigma$ manifold. The Ni−S $\pi$ bonding is also perturbed by hopping of sulfur from an axial to an equatorial position, which enhances overlap in the empty antibonding orbital (22a″) at the expense of the filled bonding orbital (20a″) and destabilizes both orbitals. The opposing effects on $\sigma$- and $\pi$-bonding yield a relatively small difference in total bonding energy between **1**′ and **5**′,

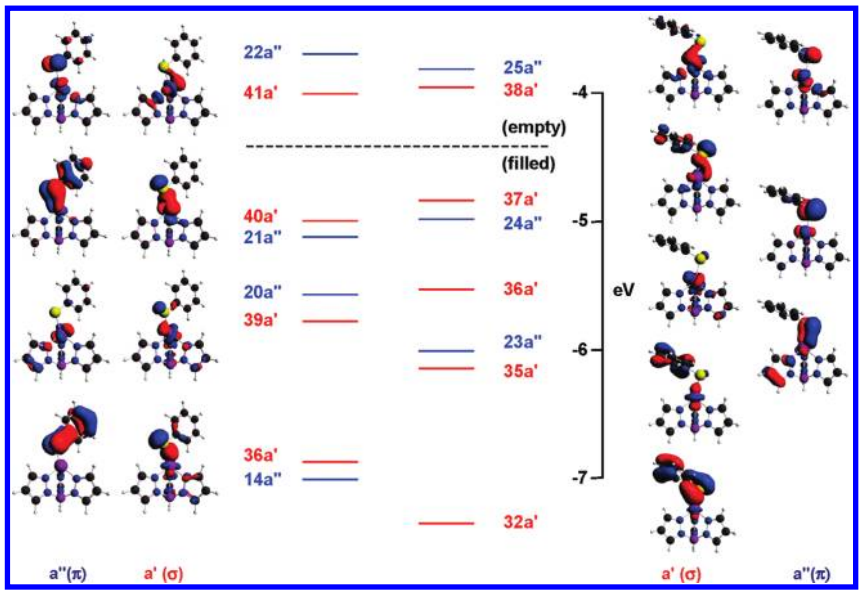


**Figure 10.** Relevant $\beta$-spin frontier orbitals for **1′** (left) and **5′** (right). Orbitals are distinguished by parity under imposed $C_s$ symmetry, with a′ (red) and a″ (blue) representations corresponding to respective $\sigma$ and $\pi$ overlap along the Ni−S bond vector.

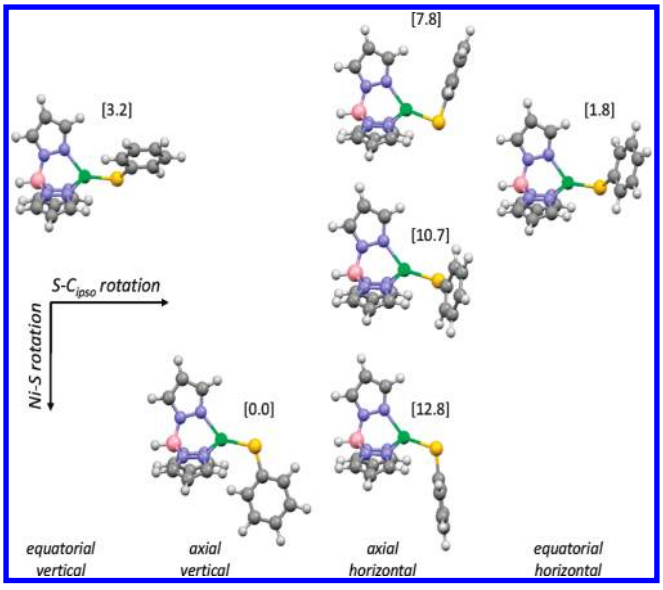


**Figure 11.** Sterically accessible limiting configurations for a simplified TpNiSPh model. Horizontal translation between columns corresponds to 90° rotation about the S−$C_{ipso}$ bond, transposing the $\pi_{ip}$ and $\pi_{op}$ thiolate donor orbitals, and vertical translation down a column corresponds to 90° rotation about the Ni−S bond, transposing Ni d$\pi$* acceptor orbitals. Number in brackets indicates the relative calculated energy in KJ/mol.

supporting a relatively flat energy surface consistent with the dynamic structural rearrangement in solution, as evidenced in NMR spectra.

**3.6.4. Conformational Energetics.** Including the respective equatorial/vertical and axial/horizontal configurations of **1′** and **5′**, a total of 16 limiting bonding configurations are possible for a bent thiolate. The sulfur can adopt axial or equatorial positions, and orthogonal rotation between the vertical and horizontal orientations exchanges the respective $\sigma$ and $\pi$ overlap symmetries of the $\pi_{ip}$ and $\pi_{op}$ donor orbitals. Furthermore, the substituent can rotate away from the Ni−S bond in 90° increments, exchanging $\pi$ overlap with orthogonal nickel d acceptor orbitals (e.g., 25a″ and 38a′ of **5′**, Figure 10); this additional factor yields the aforementioned sixteen orientations (i.e., equatorial/axial × horizontal/vertical × 0/90/180/270°). However, the 90° and 270° rotations are enantiomorphous, so only 12 configurations are energetically unique. Such rotation is evident in the structure of $PhBP_3Ni$-S-$C_6H_4$-4-$^t$Bu reported by MacBeth, et al.[15] Even for the miminal TpNiSPh models with no substituents, only six of these configurations are sterically accessible as local minima (Figure 11), excluding from consideration the thirteenth umbrella configuration, with a linear thiolate and both $\pi_{ip}$ and $\pi_{op}$ in a $\pi$-bonding orientation. Added substituents presumably would further reduce the number of assessible configurations. Optimization of the six model conformations suggests a relatively flat energy surface within 13 KJ/mol of the global minimum; the absolute accuracy is unknown, although calculations on isomeric configurations of the same complex would presumably cancel some systematic error. Three of these six configurations have been observed experimentally. Five of the seven known tripodal thiolate structures adopt the equatorial/vertical/0° configuration (Table 1),[9,13,14] which is calculated to lie only 5−8 KJ/mol below the axial/horizontal configurations adopted by **5** and $PhBP_3Ni$-S-$C_6H_4$-4-$^t$Bu.[15] Only small enhancement of steric contact at the *ortho* position should suffice to tip the minimum from the equatorial/vertical configuration observed for **1** into the axial/horizontal configuration of **5**. The modest substitution of **2**−**4** would accordingly enable equilibration between both conformations. Other configurations have yet to be observed, including an axial/vertical/180° structure identified as the global minimum for TpNiSPh. However, this configuration was recently observed in a crystal structure of a tripodal copper(II) phenolate.[48]

**3.6.5. TD-DFT Calculations and Electronic Spectra.** TD-DFT calculations were performed on models **1″** and **5′** under respective experimental $C_1$ and $C_s$ symmetry, to provide a basis for assignment of the observed CT bands already described in electronic spectra (Figure 12). The vacant $\beta$-spin orbitals of $\sigma$ symmetry (41a′ and 38a′ in

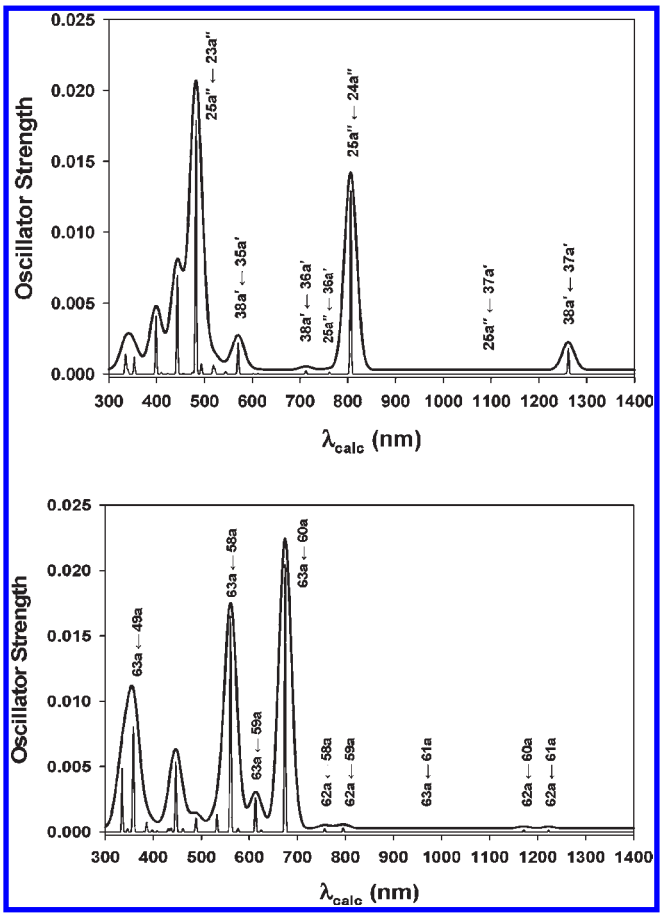


**Figure 12.** TD-DFT calculated spectra of **1**″ (bottom) and **5**′ (top). Ligand field and S−Ni LMCT bands are labeled with predominant orbital contributions. For convenience, calculated lines are presented as Gaussian curves with line widths of 3 nm (corresponding to the vertical intensity scale) and 50 nm (vertical scale exaggerated with offset).

**1**′ and **5**′, respectively) exhibit little contribution from the thiolate sulfur (3.1 and 3.7% S p, respectively). The TD-DFT calculations accordingly predict that the strongest transitions arise within the Ni−S $\pi$ bond manifolds. The next set of empty acceptor orbitals are $\pi^*$ orbitals localized on the pyrazole and arylthiolate substituent rings; as these lie 3.5−3.8 eV above the highest occupied orbitals, they would support MLCT and $\pi-\pi^*$ transitions deeper into the UV.

The three-orbital $\pi$ stack in **5**′ yields two CT excitations (Figure 12, top), one at 806 nm (25a″ ← 24a″) and the other at 482 nm (25a″ ← 23a″). Several weaker pyrazole-centered LMCT bands are calculated to fall in the range of about 400−600 nm;[49] two such transitions are evident on the high-energy side of the 482 nm LMCT band. The three most prominent ligand field bands fall at 1261, 712, and 571 nm. Calculations on **1**″ (Figure 12, bottom) also predict two strong CT bands arising from the Ni−S $\pi$ interaction at 674 (63a ← 60a, corresponding to 22a″ ← 21a″ under $C_s$ symmetry) and 560 nm (63a ← 58a), plus a third band at 359 nm arising from the $3b_2$ donor orbital (63a ← 49a; 22a″ ← 14a″). Owing to the reduced symmetry, the intermediate band is actually a ligand field transition that gains intensity by configuration interaction with the nearby CT transition (63a ← 59a; 22a″ ← 20a″) at 612 nm. The remaining features are pyrazole LMCT and ligand field bands comparable to those described for **5**′.

The calculations qualitatively reproduce the differences observed between the CT spectra of **1** and **5**, which arise from the difference in Ni−S $\pi$ overlap in their respective equatorial and axial conformations. This demonstrates that UV−visible−NIR spectroscopy can distinguish the various Ni-SAr configurations (Figure 5). The assignments just given also rationalize the comparative shifts in band energies across the Hammett series **6**−**8** (Figure 7). However, while calculated ligand field energies appear to be reasonably accurate, Ni−S LMCT energies calculated herein depart from experimental results by an average of $0.6 \pm 0.2$ eV, in line with the present state of the art.[34] The low symmetry can also enable configuration interactions, and the energies of the relevant orbitals will be perturbed by arylthilolate substitution, a continuum of possible substituent rotations, steric interactions and $\sigma^*$ interactions with the supporting tripodal ligand. Hence, while unique TD-DFT results were computed for the various limiting conformations of TpNiSPh (see Supporting Information), these may not be fully predictive of spectra for structures yet to be obtained experimentally.

## 4. Conclusions

We have elicited structurally distinct axial/horizontal and equatorial/vertical configurations for bent arylthiolate ligands at a pseudotetrahedral Ni(II) center using steric interactions. The resulting conformers can be distinguished by spectroscopy in solution, and we rationalized this result on the basis of divergent electronic structures arising from differential Ni−S $\pi$ overlap. Sterically unhindered arylthiolate ligands coordinate to a $[Tp^{Me,Me}Ni(II)]^+$ center in an equatorial position within an axially vacant trigonal bipyramidal ligand field. Steric contact from increasingly bulky *ortho* substitution displaces the arylthiolate ligand into the axial position. Limiting equatorial and axial configurations were structurally and spectroscopically defined for **1** and **5**, while complexes **2**−**4** appear to be distributed between the limiting structures in solution. Thus, the series of complexes **1**−**5** can be taken to be a steric titration, in which increasing size of the *ortho* arylthiolate disubstitution (i.e., H, Me, iPr, Ph) destabilizes preferred equatorial/vertical coordination. In contrast, sterically innocent *para* modification with substituents of varying electronic donor strength (i.e., OMe, Me, Cl) effect informative spectroscopic perturbation of CT features in **6**−**8** without altering the coordination geometry from that of **1**.

Only a handful of other pseudotetrahedral Ni(II) arylthiolate complexes have been structurally characterized, and the majority of these are tetragonally distorted (i.e., $D_{2d}$ symmetry) $[Ni(SR)_4]^{2-}$ salts.[17−20] Also noteworthy is a linear $Ni(SAr)_2$ complex.[21] The others are monothiolate complexes supported by anionic tripodal borate ligands. These examples include $PhB(CH_2PPh_2)_3Ni$-S-4-$C_6H_4Bu$,[15] $Tp^{iPr,iPr}Ni$-$SC_6F_5$,[13] $PhB(CH_2S^tBu)_3Ni$-$SC_6F_5$,[14] $PhB(CH_2S^tBu)_3Ni$-$SC_6H_5$,[14] and $Tp^{Ph,Me}Ni$-S-2,6-$Me_2C_6H_3$ (**9**).[9] The first complex was the initial example of an axial/horizontal configuration like **5**, but also uniquely twisted toward a 90° sidesaddle configuration. The arylthiolate is bent off-axis

(49) Randall, D. W.; DeBeer George, S.; Hedman, B.; Hodgson, K. O.; Fujisawa, K.; Solomon, E. I. *J. Am. Chem. Soc.* **2000**, *122*, 11620–11631.

into an equatorial/vertical orientation analogous to **1** in all the other complexes. In the last complex, the relatively large 3-Ph pyrazole moieties enforce retention of a vertical orientation even with the same *ortho* substituents as **2**.

The recent structural characterization of two Cu(II) phenolate complexes, $Tp^{iPr,iPr}Cu-O-C_6H_4$-4-F and $Tp^{tBu,iPr}$-$Cu-O-C_6H_4$-4-F, which are sterically distinguished by the proximal 3-pyrazole positions rather than substitution on the phenolate co-ligand, provides another relevant example.[48] The phenolate ligand binds axially in both complexes; however, in the $Tp^{iPr,iPr}$ complex, the substituent is again twisted toward a sidesaddle orientation, while the bulkier 3-$^t$Bu substituents force the latter complex into an axial/vertical/180° conformation. This switches phenolate donor orbitals between the complexes, and as for **1** and **5**, significant differences were observed in the electronic spectra of these complexes.

More recently, structural characterization of a pseudotetrahedral alkylperoxo complex $Tp^{iPr,iPr}Ni-OO^tBu$ was reported.[50] The Ni−O bond was displaced from the H−B···Ni axis toward one pyrazole, with the OR substituent folded back between the other two pyrazoles and approaching $\eta^2$ coordination. The geometry and bonding of this complex are analogous to equatorial/vertical arylthiolate coordination, and an axial conformation with a reversed alkylperoxo ligand can be predicted on this basis.

In concert with these results, our study suggests an expanded range of bonding configurations is accessible to arylthiolates and isolobal ligands at pseudotetrahedral metal centers. Structural characterization of disparate coordination geometries underscores the potential to elicit rich coordination chemistry by steric manipulation at the periphery of these ligand fields. As the conformers can be distinguished by routine spectroscopy, a full range of ligand configurations can be eventually observed and their effects on complex reactivity elucidated.

**Acknowledgment.** This work was supported by startup funding provided by Ohio University (M.P.J.).

**Supporting Information Available:** Miscellaneous spectroscopic data, TD-DFT spectra and Cartesian coordinates for six geometry optimized conformations of TpNiSPh (.pdf). Crystallographic data in CIF format. This material is available free of charge via the Internet at http://pubs.acs.org.

(50) Hikichi, S.; Okuda, H.; Ohzu, Y.; Akita, M. *Angew. Chem., Int. Ed.* **2009**, *48*, 188–191.